Homogenized elasticity solvers for biomorphic microcellular ceramics

R. H. W. Hoppe, S. I. Petrova

Summary. Processing of ceramic composites from biologically derived materials has recently attained particular interest. Biomorphic microcellular silicon carbide ceramics from wood with anisotropic porous microstructures pseudomorphous to wood have been produced in the last few years. The mathematical microstructural model related to the inelastic behavior of the new composite materials is formulated. The development and implementation of optimal strategies for the mechanical performance of the ceramic composites are based on a homogenized macrostructural model. The latter is obtained by assuming a periodical distribution of the microstructure treated as an infinitesimal square periodicity cell. The homogenized elasticity coefficients are computed numerically by using a finite element discretization of the cell. Efficient solution techniques for the stationary homogenized equation in the whole domain are proposed in the case of linear elasticity.

1 Introduction

Biotemplating is a new concept for preparation of ceramic composite materials with biomorphic microstructures which has attracted a great deal of interest recently. In contrast to engineering materials, biological structures exhibit a hierarchically built anatomy, developed and optimized in a long-term genetic process. Their inherent cellular, open porous morphology can be used for liquid or gaseous infiltrations and subsequently for high temperature reaction processes. For instance, wood is a natural composite which exhibits an anisotropic, porous morphology with excellent strength at low density, high stiffness, elasticity, and damage tolerance. A typical feature of wood structure is its system of tracheidal cells which provide the transportation path for water and minerals within the living tree. This open porous system is accessible for infiltration of various metals.

Among the large variety of ceramic composites, new biomorphic cellular silicon carbide (SiC) ceramics from wood were recently produced and investigated (cf., e.g., [6, 7]). The preparation of SiC ceramic materials includes two processing steps (see Fig. 1). Biological porous carbon preforms (also called C_B-templates) can be derived from different wood structures by drying and high-temperature pyrolysis at temperatures between 800 and 1800°C and used as templates for infiltrations by gaseous or liquid silicon (Si) to form SiC and SiSiC-ceramics, respectively. During high-temperature processing, the microstructural properties of the bio-organic preforms were retained, so that a one-to-one reproduction of the original wood structure was obtained. The resulting cellular composites show low density, high specific strength, and excellent high temperature stability.

The paper is organized as follows. Section 2 describes the constitutive microstructural model for the inelastic behavior of biomorphic cellular silicon carbide ceramics.

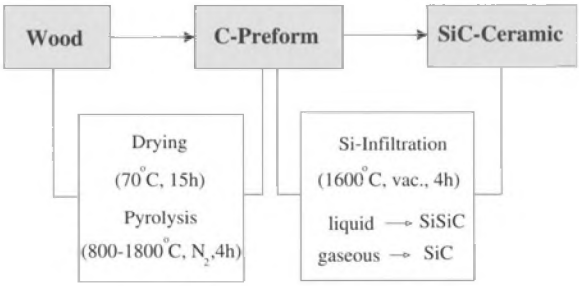

Fig. 1. Processing scheme of cellular SiC and SiSiC-ceramics from wood

In the real material model, the molecular orientation of the carbon induces a crystallographic texture of the SiC composite which strongly influences the mechanical and elastic properties of the ceramic materials. Hence, the constitutive relation has to contain a mismatch tensor due to the lattice mismatch orientations between the different phases of carbon and silicon carbide. The macroscale model obtained by using the homogenization approach is discussed in Sect. 2. We assume a periodical distribution of the composite microstructure treated as an infinitesimal square periodicity cell. The homogenized elasticity coefficients are computed numerically in the case of stationary microstructure. Efficient solution techniques applying point- and block-wise preconditioners to the stiffness matrix of the homogenized elasticity equation are tested in Sect. 3. Computational results illustrating the convergence rate of the proposed methods are presented.

2 The constitutive microstructural model

In this section, we formulate the mathematical microstructural model related to the inelastic behavior of our composite materials. We assume a sharp interface between the carbon and the silicon carbide phases in the microstructure (see Fig. 3). Referring to the theory in [1] we consider the following dynamic and constitutive equations describing the evolving microstructure:

$$-\operatorname{div}\boldsymbol{\sigma}(x,t) = \boldsymbol{f}(x,t), \tag{1}$$

$$\boldsymbol{\sigma}(x,t) = \boldsymbol{E}(s)\,(\boldsymbol{e} - \boldsymbol{e}_P - \boldsymbol{e}_M(s))\,, \tag{2}$$

$$z_t = \boldsymbol{g}(\boldsymbol{e}, \boldsymbol{e}_P, \boldsymbol{e}_M, z), \tag{3}$$

$$s_t = -v_n\,\boldsymbol{n}\cdot\nabla s, \tag{4}$$

where $\boldsymbol{\sigma}$ is the Cauchy stress tensor, $\boldsymbol{E}(s)$ is the elasticity tensor, $\boldsymbol{u}$ is the displacement vector, $\boldsymbol{e} = \boldsymbol{e}(\nabla\boldsymbol{u})$ is the linearized strain tensor, and $\boldsymbol{e}_P = Bz$ is the plastic strain tensor. Here, z stands for the vector of internal variables and B is a linear mapping. In principal, the components of $\boldsymbol{e}_P$ belong to the internal variables z. The tensor $\boldsymbol{e}_M(s) = A(s)\boldsymbol{\sigma}^m$, $m \in \mathcal{N}$, is referred to as a mismatch tensor due to the lattice

mismatch orientations between the (0001) phase of carbon and the (110) phase of SiC (cf. Fig. 2). The tensor $A(s)$ can be found experimentally. Note that (2)–(3) are the constitutive equations whereas (4) is a dynamic equation describing the evolution of the interface by means of an order parameter $s = s(x, t)$. Here, s is a jump function with values 0 or 1 indicating the location (carbon or SiC phase) of a material point x at a time t. The velocity of the interface in the normal direction $\boldsymbol{n}$ is denoted by $v_n = v_n(x, t)$. The microstructural model equations (1)–(4) have to be completed by initial and boundary conditions, inequality constraints indicating the transition from elastic to plastic behavior, and appropriate transmission conditions on the interface taking into account discontinuities and chemical reaction rates.

For scaled periodically distributed microstructures one assumes an asymptotic expansion of the solution (displacement vector) of the nonhomogenized equations (1)–(4) and obtains a macroscale homogenized model. The limit process is related to periodic structures with a size very small with respect to the size of the whole domain.

Our efforts further will be addressed to the development and implementation of optimal strategies based on the homogenized macrostructural model. The structural optimization problem for the mechanical performance of the ceramic composites will be solved subjected to specific constraints on the state variables and design parameters. In the stationary case one is often led to minimization problems of the free energy described by nonconvex energy functionals. Primal-dual Newton-type interior-point methods can be applied to the resulting nonconvex nonlinear optimization problem. For more details concerning the formulation of the optimization problem for biomorphic ceramics, see [8]. For unsteady problems with an evolving

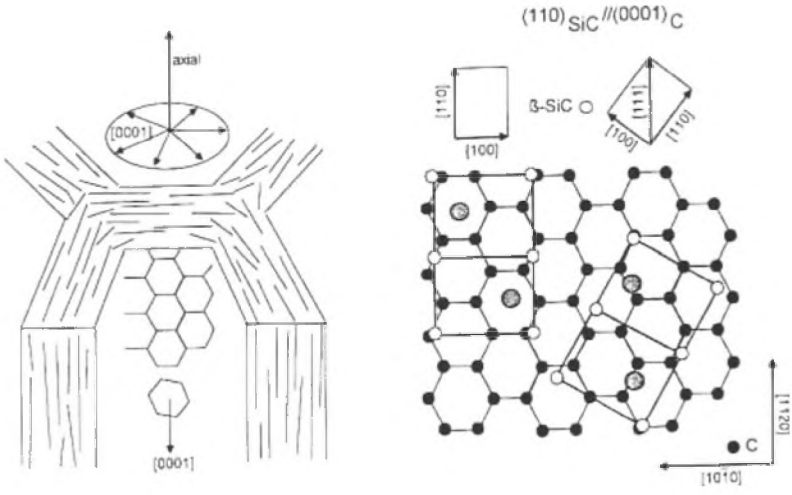

Fig. 2. Crystallographic textures of pyrolized carbon and SiC

interface between the different phases in the microstructure one has to use more complicated techniques for the temporal and spatial distribution of the interface (cf., e.g., [1]).

3 Computation of the homogenized elasticity tensor

We now discuss the application of the homogenization approach (cf., e.g., [2, 4, 9, 10]) for finding the optimal topology of a body consisting of composite microcellular SiC-ceramic material. The macroscopic material properties of the composite medium are strongly influenced by the microscopic behavior of the local periodic structure. Homogenization is possible if the macro- and micro-scales are well separated, i.e., we assume that the periodic cells in the macrostructure are infinitely many but infinitely small and repeated periodically through the medium.

We restrict ourselves to a stationary microstructure and isotropic linearly elastic constituents. Consider a two-dimensional bounded domain Ω of a composite material with a periodically distributed microstructure as shown on Fig. 3. In practice, after chemical etching, the silicon can be removed to increase the porosity, so that the porous medium can be considered as a void (no material). Hence, for the local structure we assume a square period $Y = \mathrm{V} \cup \mathrm{SiC} \cup \mathrm{C}$, where V stands for the void, SiC stands for the silicon carbide area, and C for the carbon phase.

Using the homogenization technique, the composite material medium in $\Omega \subset \mathbf{R}^2$ can be described by homogenized (effective) macroscopic material properties which depend on the geometry of the unit cell. We assume that the boundary $\partial\Omega = S_1 \cup S_2$, $S_1 \cap S_2 = \emptyset$, and meas $S_1 > 0$ and we consider the space $H := \{\boldsymbol{u} | \boldsymbol{u} \in (H^1(\Omega))^2, \boldsymbol{u}_{|S_1} = \mathbf{0}\}$.

We introduce a macroscopic (slow) variable x and a microscopic (fast) variable y. The periodicity is regarded as a small dimensionless number $\varepsilon = x/y \ll 1$ further referred to as a *scale parameter*. Assume that the macrostructure is subjected to a body force and a surface traction. Denote by $\boldsymbol{u}_\varepsilon(x) := \boldsymbol{u}(x/\varepsilon)$ the solution of the linear elasticity problem

$$-\operatorname{div} \boldsymbol{\sigma}_\varepsilon(x) = \boldsymbol{f}(x) \qquad \text{in } \Omega, \tag{5}$$

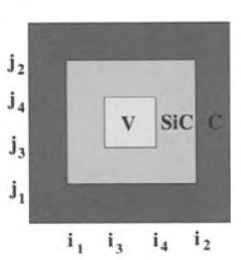

Fig. 3. The periodicity cell $Y = \mathrm{V} \cup \mathrm{SiC} \cup \mathrm{C}$

where $\boldsymbol{\sigma}_\varepsilon(x) = \boldsymbol{E}_\varepsilon(x)\boldsymbol{e}(\boldsymbol{u}_\varepsilon)$ is the stress tensor, $\boldsymbol{u}_\varepsilon$ is the displacement field, and $\boldsymbol{e}(\boldsymbol{u}_\varepsilon) = D^T\boldsymbol{u}_\varepsilon$ is the linearized strain tensor, where

$$D = \begin{pmatrix} \frac{\partial}{\partial x} & 0 & \frac{\partial}{\partial y} \\ 0 & \frac{\partial}{\partial y} & \frac{\partial}{\partial x} \end{pmatrix}.$$

The elasticity tensor $\boldsymbol{E}_\varepsilon(x) := \mathbf{E}(x/\varepsilon) = \boldsymbol{E}(y)$ is piecewise constantly defined on the periodicity cell Y. The elasticity coefficients $E_{ijkl}(y)$, $i, j, k, l = 1, 2$, are assumed to be Y-periodic functions (i.e., take equal values on opposite sides of Y). The displacement field $\boldsymbol{u}_\varepsilon$ can be expanded as

$$\mathbf{u}_\varepsilon(x) = \boldsymbol{u}^{(0)}(x, y) + \varepsilon\,\boldsymbol{u}^{(1)}(x, y) + \varepsilon^2\,\boldsymbol{u}^{(2)}(x, y) + \cdots, \tag{6}$$

where $\boldsymbol{u}^{(j)}(x, y)$ are Y-periodic in y. Under assumptions of symmetry and ellipticity of the elasticity coefficients $E_{ijkl}(y)$ it was shown (cf., e.g., [4]) that the sequence $\{\boldsymbol{u}_\varepsilon\}$ of solutions of (5) tends weakly in H, as $\varepsilon \to 0$, to the vector function $\boldsymbol{u}^{(0)}(x) \in H$, independent of y, which is the solution of the following problem defined in Ω with a constant elasticity tensor:

$$-\operatorname{div}\boldsymbol{\sigma}(x) = \boldsymbol{f}(x) \qquad \text{in } \Omega. \tag{7}$$

Here, $\boldsymbol{\sigma}(x) = \boldsymbol{E}^H\boldsymbol{e}_x(\boldsymbol{u}^{(0)})$ is the so-called *homogenized stress tensor*, $\boldsymbol{E}^H$ is the *homogenized elasticity tensor* with constant components E^H_{ijkl} (called *homogenized* or *effective* coefficients), and $\boldsymbol{u}^{(0)}(x)$ is the *homogenized displacement vector*. The homogenized elasticity tensor has the form

$$\boldsymbol{E}^H = \begin{pmatrix} E^H_{1111} & E^H_{1122} & 0 \\ E^H_{2211} & E^H_{2222} & 0 \\ 0 & 0 & E^H_{1212} \end{pmatrix}. \tag{8}$$

Using the convention of summation on repeated indices, we can write the homogenized coefficients in (8) as (see, e.g., [2, 3, 9, 10])

$$E^H_{ijkl} = \frac{1}{|Y|}\int_Y \left(E_{ijkl}(y) - E_{ijpq}(y)\frac{\partial \xi^{kl}_p}{\partial y_q}\right) dy, \tag{9}$$

where $\boldsymbol{\xi}^{kl} = \boldsymbol{\xi}^{kl}(y_1, y_2) \in [H^1(Y)]^2$ is a Y-periodic function which is considered as a microscopic displacement field for the following elasticity cell problem given in a weak formulation:

$$\int_Y \left(E_{ijpq}(y)\frac{\partial \xi^{kl}_p}{\partial y_q}\right)\frac{\partial \phi_i}{\partial y_j}\,dy = \int_Y E_{ijkl}(y)\frac{\partial \phi_i}{\partial y_j}\,dy \qquad \forall \boldsymbol{\phi} \in V_Y. \tag{10}$$

Here, V_Y is the set of all admissible Y-periodic virtual displacement fields.

Explicit formulas for the homogenized elasticity coefficients (9) can be found only in the case of layered materials and checkerboard structures (cf., e.g., [2, 3, 10]). For most geometries, however, this computation has to be done numerically. Due to the equal solutions $\xi^{12} = \xi^{21}$ one has to solve three problems (10) in the period Y with a left-hand side corresponding to the bilinear form

$$a(\xi^{kl}, \phi) = \int_Y E_{ijpq}(y)\, e_{pq}(\xi^{kl})\, e_{ij}(\phi)\, dY = \int_Y \sigma_{ij}(\xi^{kl}) e_{ij}(\phi)\, dY.$$

Problem (10) is subjected to periodic boundary conditions on ∂Y and continuity conditions $[\xi^{kl}] = 0$ and $[\sigma \cdot \boldsymbol{n}] = 0$ on the interfaces V-SiC and SiC-C. The symbol [ ] denotes the jump of the function across the corresponding interface with normal vector $\mathbf{n}$ (cf., e.g., [2]).

We now present computational results for solving (10) by using the finite element method with linear basis functions. Suppose that $Y = [0, 1] \times [0, 1]$ with a number of grid nodes on the coordinate axes Ox and Oy denoted by n_x and n_y, respectively. The computations were carried out over a regular triangular mesh with discretization parameters $h_x = 1/n_x$ and $h_y = 1/n_y$. We fix the void region by $[i_3 h_x, i_4 h_x] \times [j_3 h_y, j_4 h_y]$ for integers $1 < i_3, i_4 < n_x$, $1 < j_3, j_4 < n_y$ with $i_3 < i_4$ and $j_3 < j_4$. To define the SiC region we use integers $1 < i_1 < i_3$, $i_4 < i_2 < n_x$ and $1 < j_1 < j_3$, $j_4 < j_2 < n_y$ (see Fig. 3). Homogeneous periodic boundary conditions are imposed on ∂Y. Plane stresses, usually applicable for sufficiently thin bodies, are assumed, so that the elasticity tensor becomes

$$\mathbf{E} = \begin{pmatrix} E_{1111} & E_{1122} & 0 \\ E_{2211} & E_{2222} & 0 \\ 0 & 0 & E_{1212} \end{pmatrix} = \frac{E}{1-\nu^2} \begin{pmatrix} 1 & \nu & 0 \\ \nu & 1 & 0 \\ 0 & 0 & (1-\nu)/2 \end{pmatrix}, \tag{11}$$

where E and ν are the Young modulus and Poisson's ratio of the corresponding phase (V, SiC, C). To avoid singularity of the stiffness matrix during computations, the void has to be represented by a weak material. Both mechanical characteristics of our three materials are given in Table 1.

The preconditioned conjugate gradient (PCG) method with a block incomplete factorization matrix exploiting block-size reduction (see [5]) as a preconditioner M is applied to solve (10). We choose zero initial guess and a stopping criterion

$$(\boldsymbol{r}, M^{-1}\boldsymbol{r}) \leq 10^{-14}(\boldsymbol{r}_0, M^{-1}\boldsymbol{r}_0), \tag{12}$$

Table 1. Young's modulus E and Poisson's ratio ν

material	E(GPa)	ν
weak material	0.1	0.45
silicon carbide	410	0.14
carbon	10	0.22

Table 2. Homogenized elasticity coefficients

n_x	n_y	i_1	i_2	i_3	i_4	it_1	it_2	it_3	E^H_{1111}	E^H_{1122}	E^H_{2222}	E^H_{1212}
10	10	2	8	4	6	7	7	7	27.3+9	3.39+9	27.3+9	9.49+9
20	20	4	16	8	12	11	11	11	23.3+9	3.38+9	23.3+9	8.18+9
40	40	8	32	16	24	19	19	19	22.0+9	3.38+9	22.0+9	7.74+9
80	80	16	64	32	48	36	36	35	21.5+9	3.38+9	21.5+9	7.56+9
100	100	20	80	40	60	45	44	45	21.3+9	3.38+9	21.3+9	7.52+9
120	120	24	96	48	72	54	54	54	21.3+9	3.37+9	21.3+9	7.50+9
160	160	32	128	64	96	74	73	74	21.2+9	3.37+9	21.2+9	7.48+9
200	200	40	160	80	120	91	90	90	21.1+9	3.37+9	21.1+9	7.46+9

where $\boldsymbol{r}$ is the current residual and $\boldsymbol{r}_0$ is the initial residual when solving (10). The number of iterations for solving our three problems (to find $\boldsymbol{\xi}^{11}$, $\boldsymbol{\xi}^{22}$, and $\boldsymbol{\xi}^{12}$) are denoted, respectively, by it_1, it_2, and it_3. After finding the solutions $\boldsymbol{\xi}^{kl}$, $k, l = 1, 2$, the coefficients E^H_{ijkl} (see (9)) are computed by using the composite trapezoidal quadrature rule.

The numerical results for the homogenized elasticity coefficients (8) for various number of nodes n_x, n_y and $j_k = i_k$, $k = 1, \ldots, 4$ (cf. Fig. 3) are presented in Table 2. Note that the sizes of the three phases (V, SiC, C) in the microstructure shown on Fig. 3 are fixed in the chosen test (see the values of i_1, i_2, i_3, i_4 when varying n_x and n_y). The aim of this experiment is to obtain more precise effective coefficients when refining the mesh.

4 The homogenized equation. Numerical experiments

In this section, we present some computational results for solving the homogenized elasticity equation (7). Suppose that the structure in Ω is subjected to a macroscopic body force and a macroscopic surface traction. The finite element discretization results in the following system of linear equations to be solved numerically:

$$A\,\boldsymbol{u} = \boldsymbol{f}, \tag{13}$$

where $\boldsymbol{u}$ is the vector of unknown displacements in x- and y-coordinates and $\boldsymbol{f}$ is the discrete right-hand side of (7). The matrix A is symmetric and positive definite but not an M-matrix. Denote the corresponding displacement components by $u_k^{(x)}, u_k^{(y)}$. Two different orderings are often used in practice, namely,

$$\left(u_1^{(x)}, u_1^{(y)}, u_2^{(x)}, u_2^{(y)}, \ldots, u_n^{(x)}, u_n^{(y)}\right), \tag{14}$$

referred to as a *pointwise displacements ordering*, and

$$\left(u_1^{(x)}, u_2^{(x)}, \ldots, u_n^{(x)}, u_1^{(y)}, u_2^{(y)}, \ldots, u_n^{(y)}\right), \tag{15}$$

referred to as a *separate displacements ordering*. In the first case, the resulting stiffness matrix $A = A^{(\text{point})}$ can be seen as a discretization matrix, consisting of elements which are small 2×2 blocks. In the second case, $A = A^{(\text{block})}$ admits the 2×2 block structure

$$A = \begin{bmatrix} A_{11} & A_{12} \\ A_{21} & A_{22} \end{bmatrix}. \tag{16}$$

The PCG method is applied to solve the system (13). We propose two approaches to construct a preconditioner for A:

(1) construct a preconditioner for $A^{(\text{point})}$;
(2) construct a preconditioner for $A^{(\text{block})}$ of the type

$$M = \begin{bmatrix} M_{11} & 0 \\ 0 & M_{22} \end{bmatrix}. \tag{17}$$

Note that the diagonal blocks A_{ii}, $i = 1, 2$, in (16) are discrete analogs of the anisotropic Laplacian operators

$$A_{11} = a\frac{\partial^2}{\partial x} + b\frac{\partial^2}{\partial y}, \qquad A_{22} = b\frac{\partial^2}{\partial x} + a\frac{\partial^2}{\partial y},$$

where $a = E/(1 - \nu^2)$ and $b = 0.5E/(1 + \nu)$. This anisotropy requires special care when constructing an efficient preconditioner for the iterative solution method. Based on Korn's inequality, it can be shown that A and its block diagonal part are spectrally equivalent. The condition number of the preconditioned system depends on the Poisson ratio of the materials and the constant in Korn's inequality. The latter is related only to the shape of the domain and the boundary conditions, so that the constant of spectral equivalence is independent of the number of unknowns in the algebraic system.

We have two possibilities for constructing M in case (2).

(2a) Construct some approximations to the diagonal blocks of M (we have chosen incomplete Cholesky factorization) and use M as a preconditioner for $A = A^{(\text{block})}$ within the PCG method. For each iteration we solve problems with the approximated blocks only once.

(2b) Set $M_{ii} = A_{ii}$, $i = 1, 2$, and use an inner-outer type solution method. During each outer iteration we solve systems with A_{ii} using another (inner) iterative procedure where A_{ii} are preconditioned by other matrices. The inner solver can be considered as a *variable-step* preconditioner since its action depends on the inner stopping criteria used and, hence, it changes from one outer iteration to another.

The domain Ω is chosen to be a circle which corresponds naturally to a cross section of our original wood structure (see Fig. 4). We use MATLAB to generate

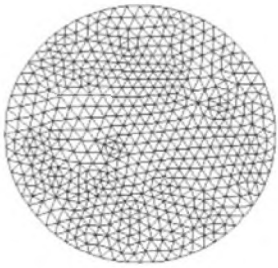

Fig. 4. Domain Ω discretized by 557 nodes

triangulation and impose homogeneous boundary conditions on the Dirichlet nodes and inhomogeneous Neumann boundary conditions on the loading surface. All computational tests were run on an Alpha PC164LX machine.

In Table 3 we report numerical results for the convergence of the iterative procedure where NN is the number of nodes, NBE is the number of boundary edges, NDN is the number of Dirichlet points, NDOF is the number of degrees of freedom (note that NDOF = 2NN − NDN), NE is the number of finite elements, ITER(P) and ITER(B) are the number of iterations to achieve accuracy, and TIME(P) and TIME(B) are the solution times given in seconds for the point and block-wise (case (2a)) preconditioners, respectively. The same stopping criterion (12) is used.

From the experimental data one can see that both preconditioners behave in a similar way when the number of degrees of freedom increases. The block-diagonal preconditioner requires more iterations to achieve convergence but it is more efficient as regards total solution time due to the elimination of the off-diagonal blocks in the preconditioning solution procedures.

Table 3. Numerical results for convergence

NN	NBE	NDN	NDOF	NE	ITER(P)	TIME(P)	ITER(B)	TIME(B)
142	32	33	251	250	23	0.63	25	0.56
369	96	144	594	640	25	1.35	27	1.23
557	64	96	1018	1048	35	3.41	41	3.29
1345	128	192	2498	2560	45	11.18	48	9.64
1631	112	168	3094	3184	56	17.32	61	17.13
1921	128	192	3650	3712	67	24.78	73	21.04
4425	208	312	8538	8704	90	80.09	99	70.35
6273	256	384	12162	12288	132	174.79	151	155.85
7553	256	384	14722	14848	135	209.65	149	183.77

Acknowledgements. This work has been partially supported by the German National Science Foundation (DFG) under Grant No.HO877/5-1. The second author is sincerely grateful to Dr. Maya Neytcheva for helpful discussions.

References

[1] Alber, H.-D. (2000): Evolving microstructure and homogenization. Contin. Mech. Thermodyn. **12**, 235–286
[2] Bakhvalov, N., Panasenko, G. (1984): Averaging processes in periodic media. (Russian). Nauka, Moscow
[3] Bendsøe, M.P. (1995): Optimization of structural topology, shape, and material. Springer, Berlin
[4] Bensoussan, A., Lions, J.-L., Papanicolaou, G. (1978): Asymptotic analysis for periodic structures. North-Holland, Amsterdam
[5] Chan, T.F., Vassilevski, P.S. (1995): A framework for the block-ILU factorizations using block-size reduction. Math. Comp. **64**, 129–156
[6] Greil, P., Lifka, T., Kaindl, A. (1998): Biomorphic cellular silicon carbide ceramics from wood: I. Processing and microstructure. J. Europ. Ceramic Soc. **18**, 1961–1973
[7] Greil, P., Lifka, T., Kaindl, A. (1998): Biomorphic cellular silicon carbide ceramics from wood: II. Mechanical properties. J. Europ. Ceramic Soc. **18**, 1975–1983
[8] Hoppe, R.H.W., Petrova, S.I. (2002): Structural optimization of biomorphic microcellular ceramics by homogenization approach. In: Margenov et al. (eds.): Large-scale scientific computing. (Lecture Notes Computer Science, vol. 2179). Springer, Berlin, pp. 353–360
[9] Hornung, U. (ed.) (1997): Homogenization and porous media. Springer, Berlin
[10] Jikov, V.V., Kozlov, S.M., Oleĭnik, O.A. (1994): Homogenization of differential operators and integral functionals. Springer, Berlin